JGR Atmospheres

RESEARCH ARTICLE
10.1029/2024JD042622

# Characteristics of the Summer Regional Precipitation Events in the Middle and Lower Yangtze River Basin and Associated Mechanisms

**Rongchang Wu[1], Anning Huang[1], Danqing Huang[1], Jian Tang[2], and Xiaoke Xu[3]**

[1]School of Atmospheric Sciences, Nanjing University, Nanjing, China, [2]National Meteorological Center of China Meteorological Administration, Beijing, China, [3]School of Geographical Sciences, Southwest University, Chongqing, China

**Key Points:**

- An objective identification method for the regional precipitation events (RPE) has been proposed
- The RPEs dominate the morning diurnal peak, interannual variation, and phased increasing trend of total precipitation in MLYRB during summer
- The summer RPEs in MLYRB mainly occur under two monsoonal synoptic types with shear line and landfalling tropical cyclone synoptic type

**Supporting Information:**

Supporting Information may be found in the online version of this article.

**Correspondence to:**

A. Huang and D. Huang,
anhuang@nju.edu.cn;
huangdq@nju.edu.cn

**Citation:**

Wu, R., Huang, A., Huang, D., Tang, J., & Xu, X. (2025). Characteristics of the summer regional precipitation events in the middle and lower Yangtze River Basin and associated mechanisms. *Journal of Geophysical Research: Atmospheres*, *130*, e2024JD042622. https://doi.org/10.1029/2024JD042622

Received 2 OCT 2024
Accepted 17 JAN 2025

**Author Contributions:**

**Conceptualization:** Rongchang Wu, Anning Huang
**Data curation:** Rongchang Wu, Jian Tang
**Formal analysis:** Rongchang Wu, Anning Huang, Danqing Huang, Jian Tang
**Investigation:** Rongchang Wu, Anning Huang, Danqing Huang, Xiaoke Xu
**Methodology:** Rongchang Wu, Anning Huang
**Resources:** Rongchang Wu, Anning Huang, Danqing Huang, Jian Tang
**Software:** Rongchang Wu
**Supervision:** Anning Huang
**Validation:** Jian Tang, Xiaoke Xu
**Visualization:** Rongchang Wu, Anning Huang
**Writing – original draft:** Rongchang Wu, Danqing Huang



**Abstract** Based on the hourly rainfall gauge data and ERA5 reanalysis data of 1980–2022, this study reveals the characteristics of regional precipitation events (RPEs) over the middle and lower Yangtze River basin (MLYRB) in summer and associated mechanisms. Results show that the RPEs contribute more than 60% of the summer total rainfall over most of MLYRB and dominate the morning diurnal peak, interannual variation, and phased increasing trend for the summer total precipitation over MLYRB. The RPEs mainly occurring under two monsoonal types with shear line (Type1 and Type2; 91.4%) and landfalling tropical cyclone type (Type3; 8.6%) show higher precipitation occurrence probability in southern/northern and eastern MLYRB. The synoptic types of summer RPEs over MLYRB show a clear sub-seasonal variation associated with the development of East Asian summer monsoon, with Type1, Type2, and Type3 concentratively occurring in June to early July (78%), late June to July (62%) and late July to August (81%), respectively. Meanwhile, the diurnal variation of RPE precipitation amount under the synoptic Type1 and Type2 (Type3) exhibits a predominant morning (afternoon) peak. Meanwhile, the increasing trend of total RPE rainfall during 1980–1999 (2000–2022) is mainly contributed by the RPEs under Type1 (Type1 and Type2 together). The reduced coverage rate and the occurrence hours of RPEs under the monsoonal synoptic types dominate the weakened diurnal variation of the RPE precipitation amount during 2000–2022 compared with 1980–1999. This study provides a new scientific reference for the differences in the characteristics of summer RPEs in the MLYRB under different synoptic types.

**Plain Language Summary** The characteristics of the summer regional precipitation events (RPEs) in the middle and lower Yangtze River Basin (MLYRB) and associated dominant synoptic types have been systematically revealed based on the hourly rain gauge data and ERA5 reanalysis data during the summers of 1980–2022. More than 60% of the summer total rainfall in most of the MLYRB is contributed by the RPEs. Meanwhile, the morning peak, interannual variation, and phased increasing trend for the total precipitation in MLYRB are controlled by the RPEs mainly occurring under two monsoonal synoptic types with shear line (Type1 and Type2) and landfalling tropical cyclone type (Type3) accompanied by the precipitation concentrated in the southern, northern, and eastern MLYRB, respectively. The synoptic types of RPEs show a clear sub-seasonal variation with the development of East Asian summer monsoon. Meanwhile, the diurnal variation of RPE precipitation amount under the monsoonal types (landfalling tropical cyclone type) exhibits a predominant morning (afternoon) peak. Moreover, the RPEs under Type1 (Type1 and Type2 together) dominate the increasing trend of the total RPE rainfall during 1980–1999 (2000–2022). This study provides a new scientific reference for recognizing the basic features of summer RPEs in the MLYRB and their differences under different synoptic types.

## 1. Introduction

Precipitation plays an important role in the distribution of water resources, natural ecosystems, water cycle, and energy budget processes in the earth system (Dagan & Stier, 2020; Korell et al., 2021; Muller & O'Gorman, 2011). In recent decades, precipitation amount and intensity have shown greater variability on the spatio-temporal scale, which poses a serious challenge to the sustainable development of human beings (Tan et al., 2023; Wang et al., 2017, 2023). Particularly, precipitation changes exhibit regional patterns under the background of global warming (Dai et al., 2024; Li et al., 2023; Muller & O'Gorman, 2011). The analysis of spatial-temporal

**Writing – review & editing:** Anning Huang, Danqing Huang, Jian Tang, Xiaoke Xu

features and associated mechanisms for regional precipitation should be strengthened, which is key to understanding the regional water cycle (Allan et al., 2020; Markonis et al., 2019).

Precipitation events can generally be categorized into regional precipitation events (RPEs) and local precipitation events (LPEs) (Guo et al., 2017; Hu & Yuan, 2021). Compared to LPEs with relatively shorter duration and smaller coverage, the RPEs with much longer duration and wider coverage are mainly induced by definite synoptic circulation patterns (Cavalcanti, 2012; Kukulies et al., 2021; Schumacher & Rasmussen, 2020; Zhang et al., 2008). Previous studies mainly focused on the evolutionary characteristics of precipitation processes at an individual station without considering the complex changes in the spatial coverage of precipitation, leading to a lack of understanding of the spatiotemporal continuum processes of precipitation events (Wang et al., 2022; Yu et al., 2015; Zhao et al., 2023). RPEs can reflect the development and decline precipitation process and revealing the formation mechanism of RPEs is of great practical significance for improving the precipitation forecasting capability (Hu et al., 2020).

As one of the rainfall centers in China, the middle and lower Yangtze River basin (MLYRB) located in the East Asian summer monsoon zone with high population density and developed economy has frequent heavy rainfall, especially during the Meiyu season (Xue et al., 2018; Yu et al., 2007). The summer rainfall in the MLYRB shows significant interannual and interdecadal variability under the influence of climate signals such as El Niño-Southern Oscillation and Pacific Decadal Oscillation on the East Asian summer monsoon (Li et al., 2021; Wen et al., 2019; Zhu et al., 2011). Qi et al. (2019) demonstrated that the interannual variation of summer precipitation has a significant positive correlation with the intensity of the intra-seasonal oscillation. However, the interannual variability of RPE rainfall and their contribution to the total rainfall remains unclear. In addition, the diurnal variation of precipitation over the MLYRB in summer exhibits a distinct bimodal character with the two-peak phase in the morning (around 8:00 LST) and late afternoon (around 18:00 LST) (Li, Furtado, et al., 2020). Meanwhile, the morning stratiform precipitation and late afternoon convective precipitation dominate the distinct characteristics of the two-peak phase precipitation (Chen et al., 2012; Yao et al., 2022; Yu et al., 2014). The eastward propagation of the synoptic system leads to the peak of precipitation diurnal phase exhibiting an eastward propagation from midnight to early morning to afternoon, which further indicates the significance of RPEs considering the spatial coverage (Wu et al., 2018; Yu et al., 2007; Zhu et al., 2023).

Persistent precipitation events occurring in the MLYRB are usually associated with typical synoptic systems that favor to enhance water vapor transport, instability of stratification, and dynamical lifting, such as quasi-stationary fronts, tropical cyclones, and eastward moving vortexes (Chen et al., 2020; Gao et al., 2023; Wu et al., 2022). Accordingly, several studies have analyzed the circulation patterns based on the typical precipitation events, indicating that the zonal propagation of Rossby wave energy from the northeast Atlantic and the northward propagation of Rossby wave packets from the western Pacific is an important mechanism to maintain the persistent precipitation in the MLYRB (Cao et al., 2019; Chen & Zhai, 2016; Wang et al., 2021). With the development of machine learning and big data analysis, the possibility of processing and analyzing a larger number of precipitation events with high temporal and spatial resolution is provided (Salcedo-Sanz et al., 2024). For instance, four typical synoptic patterns triggering the summer extreme precipitation over the middle and lower reaches of the Yangtze River are identified by hierarchical clustering, emphasizing the importance of mid-latitude weather disturbance in extreme precipitation (Hu et al., 2023). Muszynski et al. (2019) identified the atmospheric river patterns in climate data sets using topological data analysis and support vector machine methods.

Because of the limitations of single case studies about precipitation events, it is necessary to systematically identify and analyze the summer RPEs in the MLYRB over the past decades. Therefore, this study develops a method for identifying the RPEs based on previous research (Guo et al., 2017; Yu et al., 2015), and aims to answer the following questions: (a) What are the characteristics of summer RPEs in the MLYRB during 1980–2022? (b) What are the typical synoptic types that induce the summer RPEs in the MLYRB? (c) What are the differences in the features of RPEs under different typical synoptic types?

## 2. Data and Methods

### 2.1. Data

The data used in this study are listed as follows:

1. The hourly precipitation data observed at 300 gauge stations which are uniformly distributed in the MLYRB (Figure S1 in Supporting Information S1) during the summers (June to August) of 1980–2022, which are qualified and provided by China Meteorological Administration (CMA).
2. The ERA5 data set with the temporal resolution of 1 hr and spatial resolution of 0.25° × 0.25° at 37 pressure levels (Hersbach et al., 2020) produced by the European Center for Medium-Range Weather Forecasts (ECMWF), including the u-component and v-component of wind, geopotential height, and specific humidity.

### 2.2. Methods

#### 2.2.1. Identification of Regional Precipitation Events

RPEs refer to the persistent occurrence of widespread precipitation events in a given region (Hu & Yuan, 2021; Li, Li, et al., 2020). Based on the hourly precipitation data observed at 300 stations in the MLYRB (28–33°N, 110–123°E), the number of stations with simultaneous precipitation (precipitation ≥0.1 mm) at each hour during the summers of 1980–2022 is recorded as *N*, then we have a time series of the station numbers with simultaneous precipitation. Following the approach of Guo et al. (2017), an occurrence hour of RPE is detected when the *N* is larger than or equal to 60, indicating the spatial coverage of precipitation ≥20% of the MLYRB area. In this study, we detected 18,654 occurrence hours of RPE during the 43 summers. The duration of an RPE is identified by the total hours of continuous RPE (Figure 1a) and then 1,384 RPEs are detected.

Some previous studies of precipitation events have not considered removing noise precipitation independent of precipitation events (Li, Li, et al., 2020; Zhang, Han, & Yang, 2021). Identifying RPEs only according to the 20% station threshold may include some noise signals of local precipitation, such as the two precipitation stations (red dots) located in the southeastern MLYRB at start time in Figure 1b that are local (noise) precipitation independent of RPE. Although the impact of noise precipitation stations on the results is relatively small, the step of identifying and excluding noise precipitation stations is scientific in terms of the precipitation formation mechanism, which can help us capture more accurate and refined features of RPEs. Density-Based Spatial Clustering of Applications with Noise (DBSCAN) is an unsupervised machine learning method that can effectively filter noise data by setting the Epsilon-neighborhood radius (eps) and the minimum number of samples in the neighborhood (min_samples) parameters (Ester et al., 1996; Schubert et al., 2017). We apply DBSCAN to identify noise signals of local precipitation, as shown in Figure 1b, DBSCAN can accurately identify the regional precipitation and local (noise) precipitation. A schematic diagram of the complete process of identifying the RPEs is presented in Figure 1. In addition, the rest of the precipitation events are uniformly referred to as LPEs in this study.

#### 2.2.2. Clustering the Dominant Synoptic Types of the RPEs

The dominant synoptic types of the RPEs are objectively identified using the spectral clustering method, which is based on graph theory and has become very popular in recent years due to its advantages over traditional clustering methods when dealing with complex structured data sets (Donath & Hoffman, 1973; Von Luxburg, 2007). The spectral clustering first constructs a similar matrix and Laplacian matrix from the input data and then obtains the corresponding eigenvector and clusters. It has been used to identify the dominant synoptic patterns of extreme weather and climate events (Tang et al., 2021; Xu et al., 2023; Zhang et al., 2024).

To discuss the atmospheric circulations that dominate the formation of RPEs, we use the *u* and *v* components of winds at 4 levels (850, 700, 500, and 200 hPa) from the ERA5 reanalysis data during all of the RPE hours (18,654, mentioned above) over the MLYRB (28–33°N, 110–123°E) as the input data for the spectral clustering. Following Tang et al. (2021) and Xu et al. (2023), at each RPE hour, the spatial dimensions (level: 4, latitude: 21, and longitude: 53) for each wind component is first reshaped into a one-dimensional array (4 × 21 × 53 = 4,452), and then the *v* one-dimensional array is put after the *u* one-dimensional array to form the whole spatial array with the size of 8,904 (4,452 × 2). Then, for the total RPE hours of 18,654, a two-dimensional array (samples: 18,654, features: 8,904) is formed and standardized along the sample dimensions to use as input data for spectral clustering (Pedregosa et al., 2011). The main purpose of standardization is to scale the numerical range of different features (such as wind fields at 200 and 850 hPa) to the same scale, to avoid the disproportionate influence of certain features on the results due to the large range of values in the clustering process. Finally, the highest Calinski-Harabasz score is used to determine the number of clusters for spectral clustering (Caliński & Harabasz, 1974). In summary, we use meridional and zonal winds on four levels as circulation features for RPE to obtain clustering results that could reflect synergistic configurations of high and low levels in the troposphere.

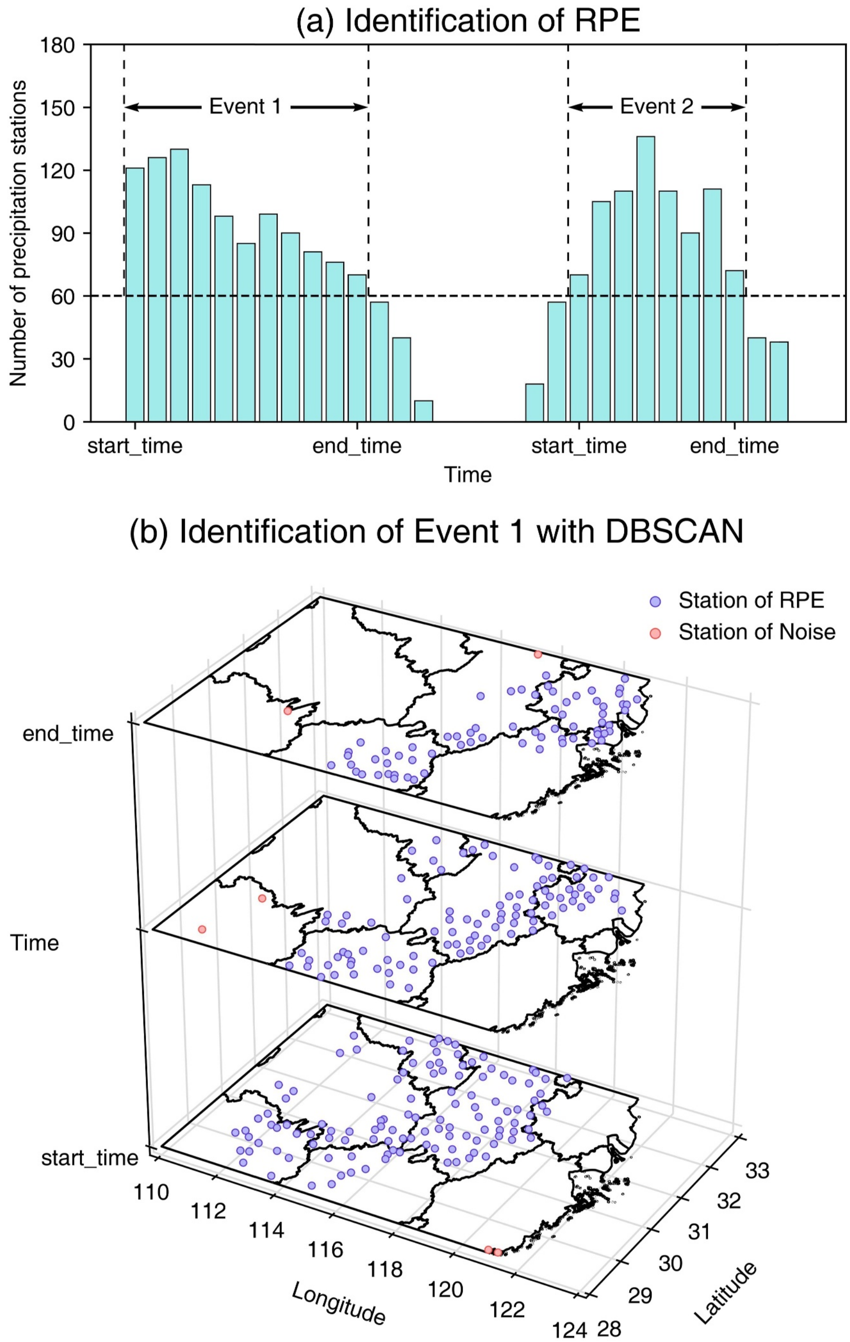


**Figure 1.** (a) Hourly time series of the number of precipitation stations during a regional rainfall event (RPE), which is detected by a threshold greater or equal to 60 stations (20% of the total stations in the MLYRB). (b) Schematic for identifying the RPE 1 using the Density-Based Spatial Clustering of Applications with Noise (DBSCAN). Purple (red) dots represent stations with precipitation belonging to regional precipitation (noise stations with precipitation) at a given hour of a RPE.

### 2.2.3. Metrics for the RPEs and Their Associated Synoptic Types

We defined three attributes of RPEs: precipitation intensity (the precipitation regionally averaged among the stations with precipitation during each RPE), coverage rate (ratio of the total numbers of stations with precipitation at each hour of a RPE to the total rain gauge stations of 300 in MLYRB), and duration (the number of hours from the start time to the end time of a RPE). For a RPE, we define the start time as $t_1$ and the end time as $t_2$, the number of stations with precipitation at the $t^{th}$ hour between the start time and end time of a RPE as

$N_t$ $(t = t_1, \cdots, t_2)$, and the rainfall at the $i^{th}$ station among the number of stations with precipitation ($N_t$) for the $t^{th}$ hour during the RPE duration as $r_{i,t}$ $(i = 1, 2, \cdots, N_t)$, and the equations for the three attributes are as follows:

$$\text{Precipitation intensity} = \frac{\sum_{t=t_1}^{t_2}\left(\sum_{i=1}^{N_t} r_{i,t}\right)}{\sum_{t=t_1}^{t_2} N_t} \quad (1)$$

$$\text{Coverage rate} = \frac{\sum_{t=t_1}^{t_2} N_t}{300 \times \text{Duration}} \times 100\% \quad (2)$$

$$\text{Duration} = t_2 - t_1 + 1 \quad (3)$$

The regional mean accumulative rainfall of an RPE is the product of precipitation intensity, coverage rate, and duration as follows:

$$\text{Rainfall} = \frac{\sum_{t=t_1}^{t_2}\left(\sum_{i=1}^{N_t} r_{i,t}\right)}{300} \quad (4)$$

In addition, the accumulated RPE or total precipitation over the MLYRB for each hour of a day during the 43 summers is divided by 3,956 hr (43 summers × 92 days in each summer) and 300 stations to obtain the time series of regional mean RPE or total precipitation amount with the sample size of 24 (24 hr of a day), which reflect the diurnal variation of precipitation amount (Wu et al., 2018). The sum of RPE precipitation intensity or coverage rate for each hour of a day during the 43 summers is divided by the total occurrence hours for each hour of a day during the 43 summers to obtain the time series of precipitation intensity or coverage rate with the sample size of 24 (24 hr of a day), which reflect the diurnal variation of RPE precipitation intensity or coverage rate. The sum of PRE precipitation occurrence hours for each hour of a day during the 43 summers to obtain the diurnal variation of RPE occurrence hours.

Furthermore, we focus on several important atmospheric circulation systems at different levels, including the shear line at 850 hPa, the South Asian high (SAH; represented by the 12,500 gpm contour at 200 hPa), the Western Pacific subtropical high (WPSH; represented by the 5,880 gpm contour at 500 hPa), and East Asian subtropical jet axis (EASJ; represented by the maximum westerly winds in the mid-latitudes at 200 hPa) (Liu et al., 2023; Ren et al., 2013; Wei et al., 2014). The shear line is a discontinuity line of wind with cyclonic shear in a low-level wind field. In this study, the identification of shear lines is based on Ma & Yao. (2015), and the meridional shear of zonal winds, relative vorticity, and the zero line of zonal wind are used to identify the shear lines at 850 hPa over the MLYRB. It is calculated as:

$$\begin{cases} \dfrac{\partial u}{\partial y} < 0 \\ \dfrac{\partial v}{\partial x} - \dfrac{\partial u}{\partial y} > 0 \\ u = 0 \end{cases} \quad (5)$$

where $u$ and $v$ are the zonal wind and meridional wind, respectively, $x$ and $y$ are the longitude and latitude.

## 3. Results

### 3.1. Characteristics of RPEs Over the MLYRB in Summer

The climatic mean summer rainfall over the MLYRB during 1980–2022 generally decreases from southeast to northwest and exhibits a relatively stronger rainfall center with the intensity exceeding 620 mm located in the hilly and mountainous areas of central MLYRB (Figure 2a). The climatic mean summer RPE rainfall exceeds 200 mm in most of the MLYRB with a southwest-northeast orienting axis of the rainfall center located in the central MLYRB (Figure 2b), which resembles the spatial distribution of the RPE occurrence hours (Figure 2c). Meanwhile, the RPEs contribute to more than 60% to the total summer rainfall in most of the MLYRB with a center larger than 70% located in the central MLYRB (Figure 2d).

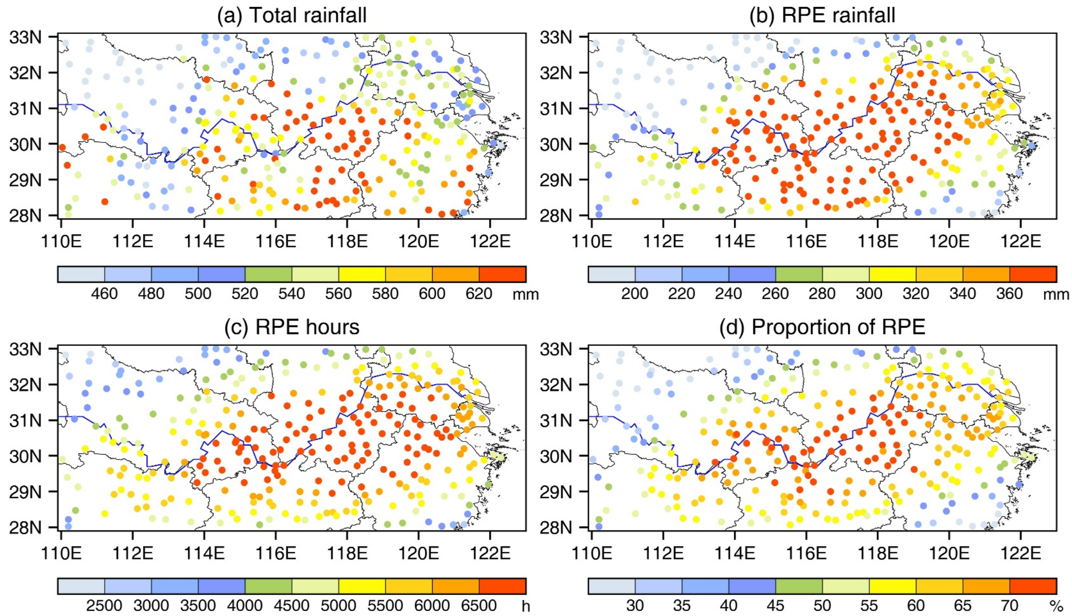


**Figure 2.** Spatial distribution of climatic mean summer total rainfall (a) and RPE rainfall (b) in the MLYRB during 1980–2022. (c) Spatial distribution of total RPE occurrence hours in the MLYRB in summer during 1980–2022. (d) Spatial distribution of the proportion of RPE rainfall to the total rainfall in summer.

As shown in Figure 3a, the diurnal variation of the RPE precipitation amount in the MLYRB exhibits two diurnal peaks featured by a predominant morning peak at around 8:00 local solar time (LST) and a secondary peak around 17:00 LST. Similar to the RPE precipitation amount, the diurnal variation of total precipitation amount also displays a clear bimodal structure, but features by a predominant peak in late afternoon and a secondary peak in morning. Overall, the morning (late afternoon) peak of the total precipitation amount over the MLYRB in summer is mainly controlled by the RPEs (LPEs) (Figure 3a). Furthermore, as shown in Figure 3b, the DBSCAN mainly excludes the local convective precipitation in the late afternoon, thus slightly reducing the late afternoon precipitation amount peak of the identified RPEs, further justifying the validation of the methodology for identifying the RPEs in this study. Although the impact of removing or not removing local (noise) precipitation by using DBSACN on the results is relatively small, the triggering mechanisms for regional precipitation and local (noise) precipitation are different, and thus removing the impact of local (noise) precipitation stations on RPEs is necessary.

As shown in Figure 3c, both the total and RPE rainfall in summer over the MLYRB show a very weak long-term trend during 1980–2022, this is mainly due to the presence of a sudden change around 2000 (Figure 3d), which may be attributed to the combined effects of interdecadal signals such as the Pacific Decadal Oscillation and Atlantic Multidecadal Oscillation (Liu et al., 2023; Zhu et al., 2011). However, it is noted a clear increasing trend in the RPE rainfall during 1980–1999 (2000–2022) at a rate of 58.53 (65.14) mm decade$^{-1}$, which mainly contributes to the trend of the total rainfall during the same period, especially during 1980–1999 the increasing trend of RPE rainfall is very close to that of the total rainfall. Meanwhile, the RPE rainfall shows a faster increasing rate than the total rainfall during 2000–2022, this is mainly resulted from the decreasing trend of the LPE rainfall (Figure 3e). In addition, the correlation coefficient between the RPE (LPE) rainfall and the total rainfall over the MLYRB in summers of 1980–2022 is 0.94 (0.11) (Figures 3c and 3e), indicating that the interannual variation of the total rainfall is mainly induced by the RPE rainfall. Overall, the interannual variation and phased increasing trend of the total rainfall over the MLYRB are mainly dominated by the RPEs, implying the importance of RPE rainfall for the total rainfall.

Figures 4a–4c show the interannual variation of precipitation intensity, coverage rate, and duration for the RPEs in summer over the MLYRB. With the atmospheric water holding capacity increasing in the context of global warming, the RPE precipitation intensity increases significantly at a rate of 0.07 mm·h$^{-1}$ decade$^{-1}$ during 1980–2022, especially with a much faster increasing rate (0.19 mm·h$^{-1}$ decade$^{-1}$) during 2000–2022 (Figure 4a), as

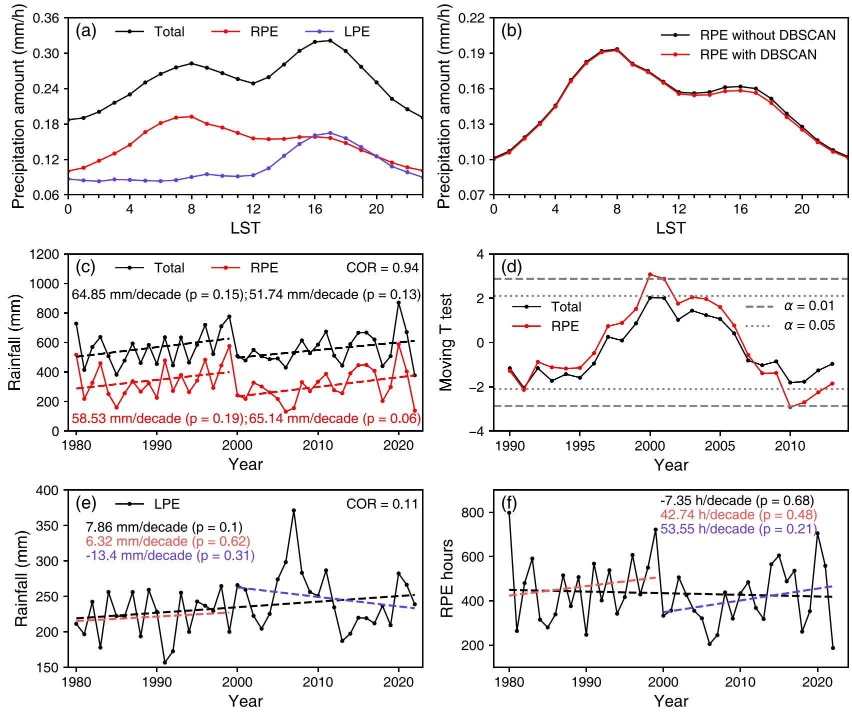


**Figure 3.** (a) The diurnal variation of the total (black line), RPE (red line), and LPE (purple line) precipitation amount. (b) The diurnal variation of precipitation amount for the RPEs identified with/without DBSCAN. (c) Time series of the total and RPE rainfall in summer regionally averaged over the MLYRB during 1980–2022. The long-term trends of the total (RPE) rainfall during 1980–1999 and 2000–2022 with associated p-values indicated by the black (red) texts. (d) 10 years moving *t*-test for the sudden change of the summer total and RPE rainfall in the MLYRB during 1980–2022. The gray dashed and dotted lines represent 0.01 and 0.05 significance level. (e) Time series of the LPE rainfall in summer regionally averaged over the MLYRB during 1980–2022. (f) Time series of RPE occurrence hours over the MLYRB in each summer of 1980–2022. The black, red, and purple texts in (e) and (f) indicate the linear trends of LPE rainfall and RPE occurrence hours during 1980–2022, 1980–1999, and 2000–2022 and associated P-values, respectively.

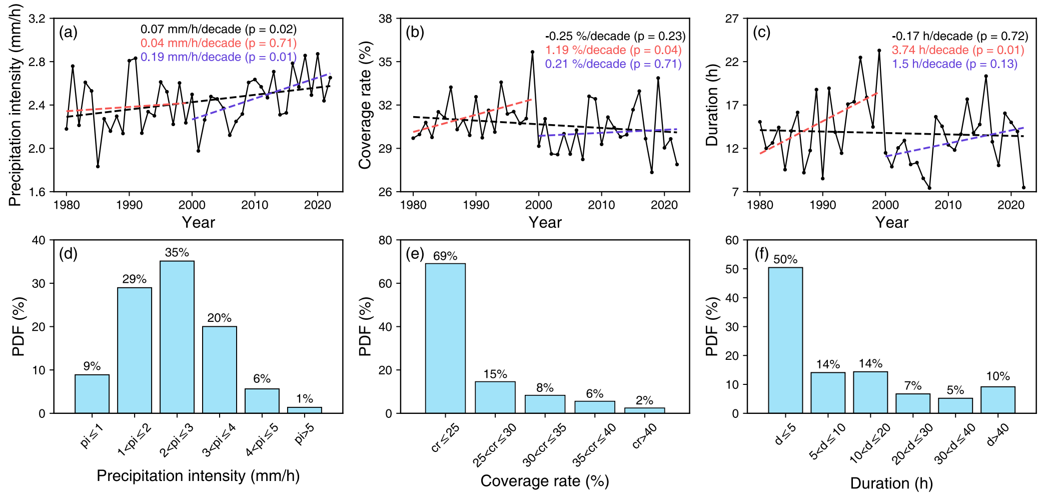


**Figure 4.** Time series of precipitation intensity (a), coverage rate (b), and duration (c) for the RPEs in summer over the MLYRB during 1980–2022 with the black, red, and purple texts indicating the linear trends of 1980–2022, 1980–1999, and 2000–2022 and associated P-values, respectively. The probability density function (PDF) of the RPE precipitation intensity (d), coverage rate (e), and duration (f).

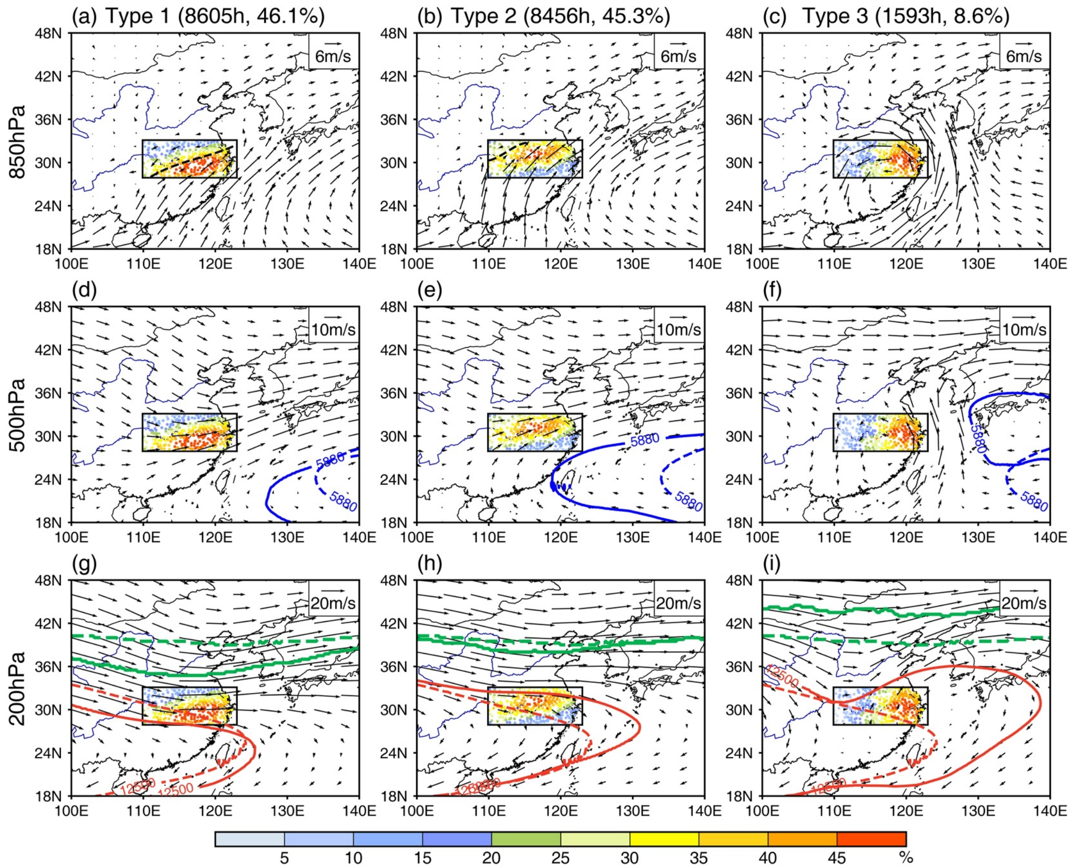


**Figure 5.** The wind field (vector) at 850 hPa (a–c), 500 hPa (d–f), and 200 hPa (g–i) under the three dominant synoptic types of RPEs identified by the spectral clustering. The shear line at 850 hpa is indicated by the black dashed line (a–b). The West Pacific subtropical high (WPSH) at 500 hPa (blue, (d)–(f)), the South Asian high (SAH) at 200 hPa (red, (g)–(i)), and the East Asian subtropical jet axis (EASJ) at 200 hPa (green, g-i) averaged during the RPEs are indicated by the solid lines, and the climatic mean WPSH, SAH, and EASJ during 1980–2022 are shown by the dashed lines. Spatial distribution of the precipitation occurrence probability (ratio of the precipitation occurrence hours at a given station under a given synoptic type to the total occurrence hours of this synoptic type) in the MLYRB under different synoptic types (a–i). The synoptic type, occurrence hours of each synoptic type and their ratios of the total occurrence hours of RPEs are shown in the title. The black box indicates the MLYRB.

reported in previous studies (Gu et al., 2020; Wu, Yin, et al., 2024). It is noted that there is a sudden change around 2000 for the RPE coverage rate and duration (Figures 4b and 4c), the sudden change in the duration directly leads to the sudden change in the RPE occurrence hours (Figure 3f) and RPE rainfall around 2000 (Figure 3c). Meanwhile, it can be noted that both the RPE precipitation intensity (Figure 4a) and occurrence hours (Figure 3f) increase at a faster rate during 2000–2022 than during 1980–1999, leading to the RPE rainfall increasing at a faster rate during 2000–2022 (Figure 3c). To further reveal the basic features of the RPEs, Figures 4d–4f give the probability density function (PDF) of the RPE precipitation intensity, coverage rate, and duration. It is clear that most of the RPEs have precipitation intensity ranging from 1 to 4 mm·h$^{-1}$ (84%), the coverage rate between 20% and 30% (84%), and the duration ≤20 hr (78%). To gain insight into the formation mechanism of the RPEs, we use spectral clustering methods to identify the dominant synoptic types during the RPEs and further reveal the basic features of RPEs under different synoptic types in the following sections.

### 3.2. The Dominant Synoptic Types Triggering RPEs Over the MLYRB in Summer

Based on the Calinski-Harabasz score (Caliński & Harabasz, 1974), three dominant synoptic types (Figure S2 in Supporting Information S1) responsible for the RPEs over the MYLRB in summer are identified by the spectral clustering method: a shear line imbeded in the East Asian summer monsoon (EASM) located over the southern (Figure 5a, Type1) or northern (Figure 5b, Type2) MLYRB, and landfalling tropical cyclone located in the eastern

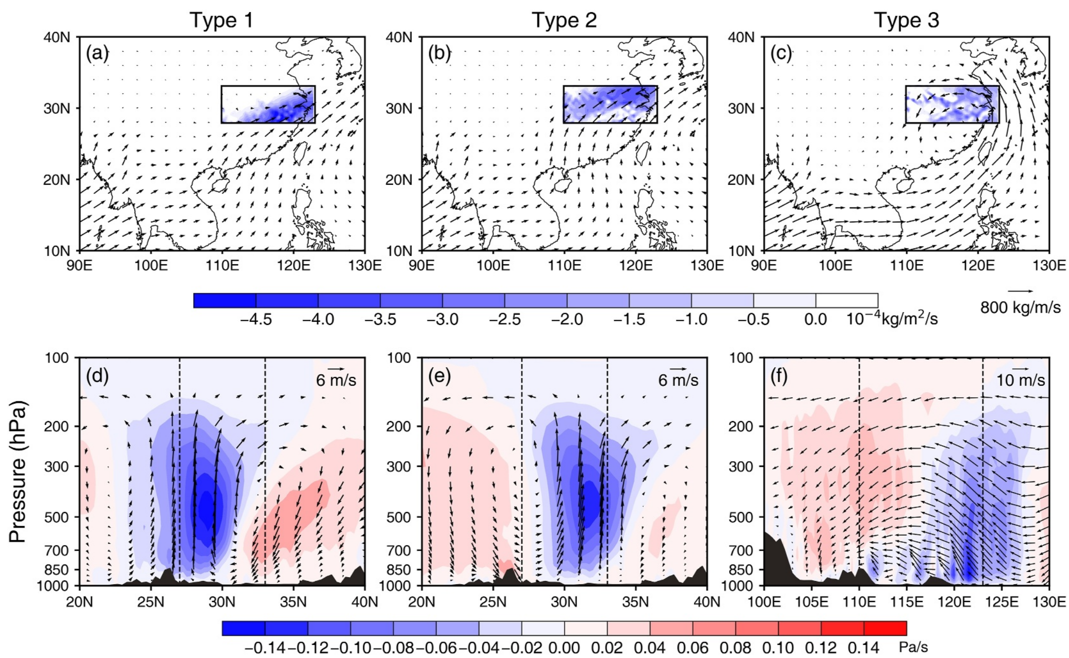


**Figure 6.** The column-integrated (from surface to 300 hPa) water vapor transport flux (vector) and its divergence (shaded) under different synoptic types (a–c). The pressure-latitude (d), (e)/longitude (f) cross sections of the anomalies of vertical velocity (shaded) and atmospheric circulation (vector) averaged along 110–123°E/28–33°N under different synoptic types relative to the climatology (d–f). The black shading in (d–f) represents the topography.

MLYRB (Figure 5c, Type3). Overall, the monsoonal types (Type1 and Type2) and landfalling tropical cyclone type (Type3) lead to 91.4% and 8.6% of the total RPE occurrence hours, respectively (Figures 5a–5c). Under the synoptic Type1, a shear line imbeded in the EASM at 850 hPa located over the southern MLYRB (Figure 5a) with the WPSH, SAH, and EASJ located southward relative to the climatology (Figures 5d and 5g) favor the convergence in lower troposphere and divergence in the middle to upper troposphere over the southern MLYRB. Meanwhile, the abundant water vapor is transported in a southwesterly path from the Bay of Bengal and the South China Sea to southern MLYRB (Figure 6a), further leading to strong moisture convergence (Figure 6a) and upward motion (Figure 6d) over the southern MLYRB and much higher precipitation occurrence probability there (Figure 5a).

Under the synoptic Type2, the configurations of the atmospheric circulations from lower to upper troposphere are featured by strong prevailing southwesterly winds over the MLYRB at 850 hPa accompanied by a shear line located over the northern MLYRB (Figure 5b), northwestward shift of WPSH at 500 hPa (Figure 5e), northeastward extension of SAH and slightly southward shift of EASJ at 200 hPa relative to the climatology (Figure 5h), this is conducive to the convergence in lower troposphere and divergence in the middle to upper troposphere over the northern MLYRB, leading to strong moisture convergence (Figure 6b) and ascending motion (Figure 6e) over the northern MLYRB and much higher precipitation occurrence probability there (Figure 5b). The synoptic Type3 is associated with the landfalling tropical cyclones, the prevailing southeasterly winds along the northeast edge of tropical cyclone at 850 and 500 hPa (Figures 5c and 5f) intensify the water vapor transport from the Northwest Pacific to the MLYRB and strengthen the moisture convergence (Figure 6c) and ascending motion (Figure 6f) over the eastern MLYRB, resulting in much higher precipitation occurrence probability there (Figure 5c).

### 3.3. The Features of RPEs Under Different Synoptic Types and Their Differences

As shown in Figures 7a–7c, the climatic mean RPE rainfall in summer over the MLYRB under the synoptic Type1, Type2, and Type3 exhibits a high rainfall center located in the southern, northern, and eastern MLYRB, respectively, which matches well with the high precipitation occurrence probability center under each synoptic type (Figures 5a–5c), indicating that the rainfall center under a given synoptic type corresponds well to the

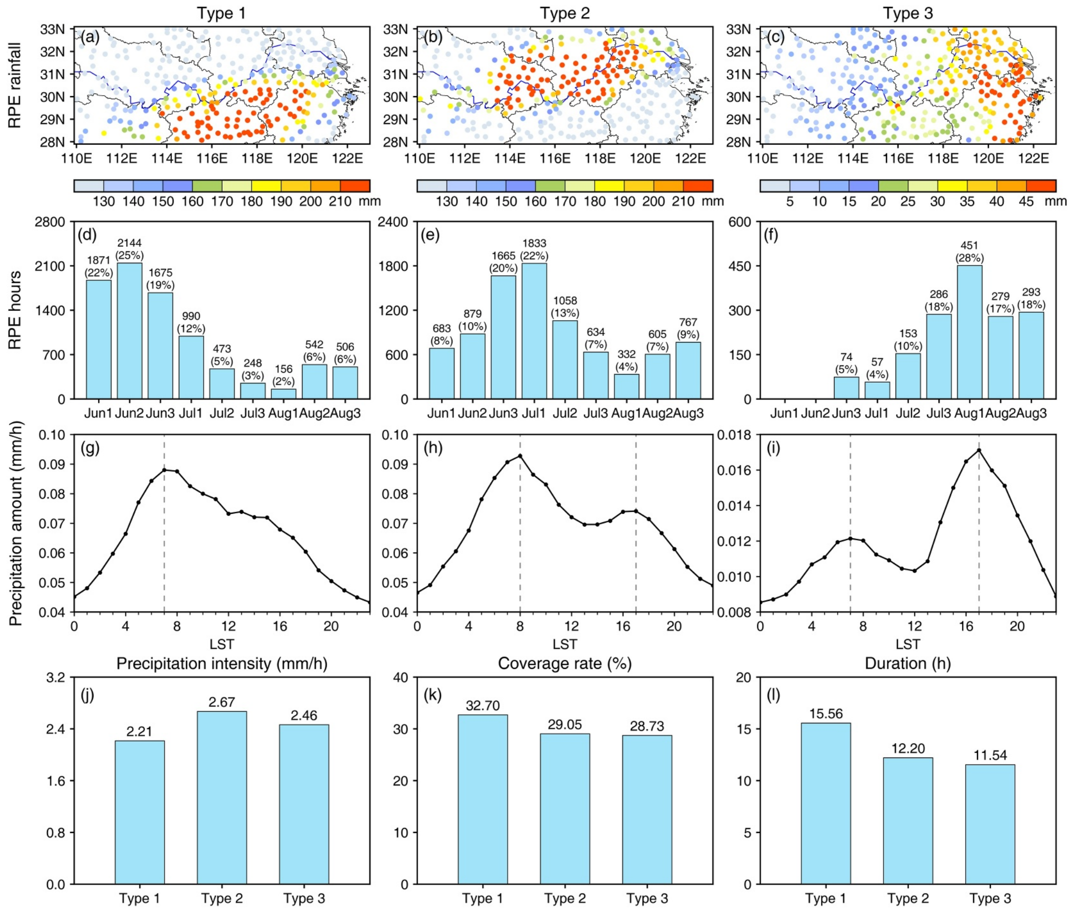

**Figure 7.** Spatial distribution of the RPE rainfall over the MLYRB in summer under different synoptic types (a–c). The sub-seasonal variation of RPE occurrence hours under different synoptic types ((d)–(f), each month is divided into three parts in units of 10 or 11 days, denoted by 1, 2, and 3). Diurnal variation of summer RPE precipitation amount under different synoptic types regionally averaged over the MLYRB, and the gray dashed line is the reference line for diurnal peak (g–i). The mean precipitation intensity, coverage rate, and duration of RPE under different synoptic types (j–l).

configurations of atmospheric circulation between the lower and upper troposphere that favors the formation of RPEs (Figure 5). Meanwhile, the dominant synoptic types responsible for the RPEs over the MLYRB display a clear sub-seasonal variation (Figures 7d–7f): the monsoonal synoptic Type1 and Type2, and landfalling tropical cyclone synoptic Type3 concentratively occur in June to early July (78%), late June to July (62%) and late July to August (81%), respectively, this is well corresponding to the sub-seasonal northward movement of EASM.

Furthermore, the diurnal variation of RPE precipitation amount under Type1 exhibits a single peak structure in the early morning (Figure 7g), suggesting that it is basically due to the stratiform precipitation (Yu et al., 2014). The diurnal variation of RPE precipitation amount under Type2 and Type3 is featured by a clear bimodal structure (Figures 7h and 7i), and a predominant peak under the synoptic Type2 (Type3) appears at 08:00 (17:00) LST. Due to the synoptic Type2 mainly occurs in the high summer (Figure 7e) when the convective activity is relatively stronger, a secondary peak of RPE precipitation occurs in late afternoon (Zeng et al., 2023). Under the synoptic Type3 associated with the landfalling tropical cyclones occurring mainly in late July and August (Figure 7f), the strong easterly water vapor transport and the low-level atmospheric instability induced by the afternoon solar heating (Li et al., 2022; Tang et al., 2019) result in the predominant peak of the RPE precipitation amount occurring in late afternoon (Figure 7i). From Figure 7j, the PRE precipitation intensity is 0.46 (0.25) mm·h$^{-1}$ stronger under the synoptic Type2 (Type3) than under the Type1 with an enhancement of 21% (11%); however, the coverage rate and duration of RPE under the Type1 (Type3) are the largest and longest (smallest and shortest) among the three synoptic types (Figures 7k and 7l).

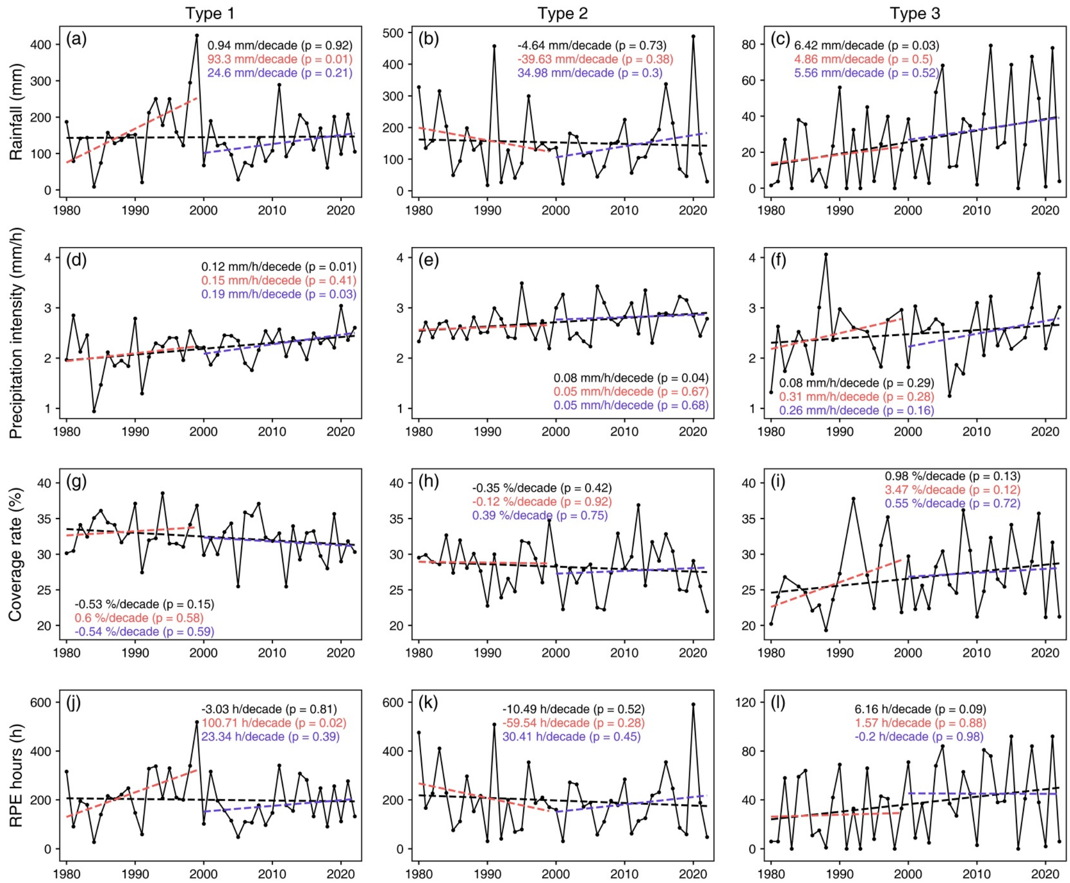


**Figure 8.** Time series of the RPE rainfall (a–c), precipitation intensity (d–f), coverage rate (g–i), and occurrence hours (j–l) under different synoptic types regionally over the MLYRB in each summer of 1980–2022. The black, red, and purple texts indicate linear trends of 1980–2022, 1980–1999, and 2000–2022 and associated P-values, respectively.

### 3.4. The Differences of RPEs Before and After the Sudden Change Around 2000

We further analyze the changes in RPEs under different synoptic types before and after the sudden change around 2000. The increasing trend of RPE rainfall during 1980–1999 (2000–2022) is mainly controlled by the RPE rainfall under the synoptic Type1 (Type1 and Type2 together) (Figures 8a and 8b), despite that in both periods the landfalling tropical cyclone induced rainfall show slight increasing trend (Figure 8c), which is attributed to an increase in the intensity and translation distance of tropical cyclones in the context of global warming (Emanuel, 2005; Qin et al., 2024). The RPE rainfall under the synoptic Type1 (Type2) before 2000 shows an increasing (a decreasing) trend, which results in the more heterogeneous spatial distribution of the long-term trends of RPE rainfall in the MLYRB during 1980–1999 compared to the period of 2000–2022 when the RPE rainfall under all synoptic types shows an increasing trend. In addition, the RPE precipitation intensity is significantly increasing under all synoptic types during all periods (Figures 8d–8f), while the long-term trend in the RPE coverage rate is increasing only under synoptic Type3 (Figures 8g–8i). Overall, the long-term trends in the RPE occurrence hours (Figures 8j–8l) and RPE rainfall (Figures 8a–8c) under each synoptic type are generally consistent, suggesting that the RPE rainfall under each synoptic type is dominated by the occurrence hours of this synoptic type. Since the atmospheric circulation under the Type1 and Type2 are characterized by the southward shift of the EASJ and the opposite zonal shift of the WPSH and SAH, respectively, the RPE rainfall may be correlated with the interdecadal variability of configures of the three systems. The opposite long-term trends of RPE rainfall under Type2 (Figure 8b) during the two periods (1980–1999 vs. 2000–2022) are possibly due to the weakening (strengthening) of SAH and WPSH intensity before (after) 2000 (Li et al., 2024; Zhang, Huang, et al., 2021).

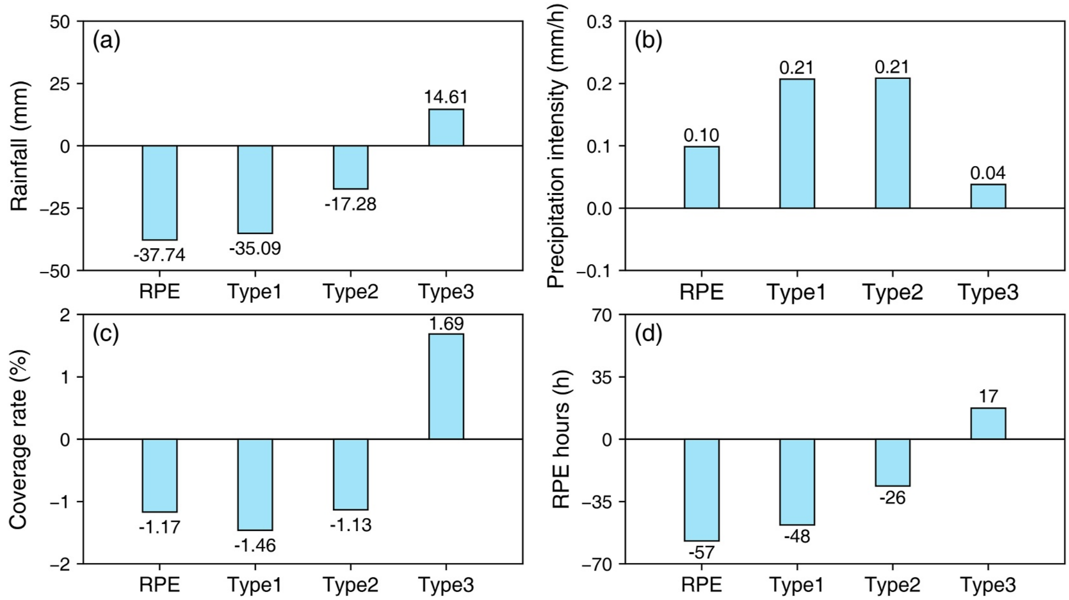


**Figure 9.** Differences in the RPE rainfall (a), precipitation intensity (b), coverage rate (c), and occurrence hours (d) between 2000-2022 and 1980–1999.

Compared with the situations during 1980–1999, despite that the landfalling tropical cyclone induced RPE rainfall strengthens due to the increased RPE precipitation intensity, coverage rate, and occurrence hours over the MLYRB in summer under the synoptic Type 3 during 2000–2022 (Figure 9), the weakened total RPE rainfall in summer during 2000–2022 is mainly resulted from the weakened RPE rainfall under both the synoptic Type1 and Type2, which is dominantly caused by the reduced RPE coverage rate and occurrence hours (Figures 9c and 9d) and may be attributed to the weakened EASJ unfavorable for inducing and sustaining RPEs due to the shift in the Pacific Decadal Oscillation phase around 2000 (Huang et al., 2013; Wu, Zhang, et al., 2024; Zhu et al., 2011).

The differences in the diurnal variation of RPEs between 2000-2022 and 1980–1999 are shown in Figure 10, compared with 1980–1999, under all of the dominant synoptic types of summer RPEs over the MLYRB, the RPE precipitation intensity during 2000–2022 is intensified at almost all hours of a day (Figures 10e–10h). However, under the synoptic Type1 and Type2 (Type3), the RPE precipitation amount (Figures 10a–10d), coverage rate (Figures 10i–10l), and occurrence hours (Figures 10m–10p) at each hour of a day are lower (higher) during 2000–2022 than during 1980–1999. Overall, the differences in the RPE precipitation amount, precipitation intensity, coverage rate, and occurrence hours between 2000-2022 and 1980–1999 at most hours of a day are much smaller under the synoptic Type3 than under both Type1 and Type2, the reduced RPE coverage rate and the occurrence hours under the monsoonal synoptic types (Type1 and Type2) dominate the weakened diurnal variation of the total RPE precipitation amount during 2000–2022 compared to 1980–1999.

## 4. Conclusion and Discussion

In this study, we developed a new objective approach to identify the RPEs based on the proportion of precipitation stations in a given region combined with the DBSCAN. The method captures the fine-scale features of RPEs and is readily applicable to the study of most weather events. Based on the hourly gauge observed precipitation data of 300 stations in the MLYRB during the summers of 1980–2022, we detected 1384 RPEs, which contribute more than 60% of the summer rainfall in most of the MLYRB. The RPE precipitation amount over the MYLRB in summer shows a bimodal structure diurnal variation featured by a predominant morning peak and a secondary late afternoon peak, and dominates the morning peak of diurnal variation of total precipitation amount. In addition, the RPE rainfall dominates the interannual variability of total rainfall over the MLYRB in summer and exhibits a faster increasing rate after 2000 than before 2000.

Based on the spectral clustering, the summer RPEs in the MLYRB mainly occur under two monsoonal types (Type1 and Type2) and landfalling tropical cyclone type (Type3). The East Asian summer monsoon with a shear

10.1029/2024JD042622

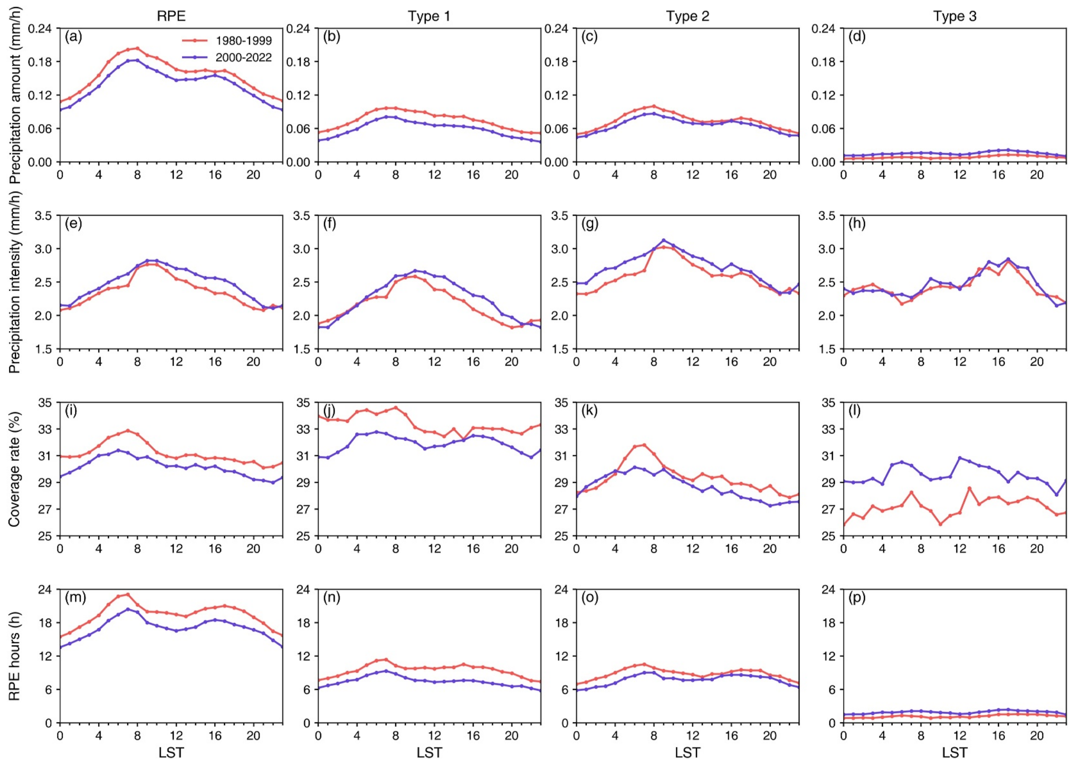


**Figure 10.** Diurnal variation of precipitation amount (a–d), precipitation intensity (e–h), coverage rate (i–l), and occurrence hours (m–p) for all of the RPEs (first column) and the RPEs under different synoptic types (second to fourth columns) over the MLYRB in summer during 1980–1999 and 2000–2022.

line imbeded in the southern or northern MLYRB (landfalling tropical cyclone located in the eastern MLYRB) leads to 91.4% (8.6%) of the total RPE occurrence hours in summer accompanied by a high precipitation occurrence probability center in the southern or northern (eastern) MLYRB. Under the Type1 (Type2), the strong southwesterly flow combined with the shear line at 850 hPa over the southern (northern) MLYRB and the southward shift of the EASJ at 200 hPa (opposite zonal shift of WPSH and SAH) is conducive to the convergence in the lower troposphere and divergence in the middle to upper troposphere and thereafter high precipitation probability there. The synoptic types of RPEs show clear sub-seasonal variations: Type1, Type2, and Type3 concentratively occur in June to early July (78%), late June to July (62%), and late July to August (81%), respectively. The advancing and retreating at sub-seasonal scales of key circulation systems, such as the EASJ, WPSH, and SAH, jointly influence the location and intensity of RPE rainfall over the MLYRB in summer (Guan et al., 2019; Yang et al., 2014).

The morning diurnal peak of RPE precipitation amount under monsoonal synoptic types (Type1 and Type2) may be associated with the stratiform precipitation, while the late afternoon diurnal peak of RPE precipitation amount under the synoptic Type3 is similar to the characteristics of the diurnal variation before the tropical cyclones landfall (Li et al., 2022; Yu et al., 2014). Moreover, the increasing trend of RPE rainfall during 1980–1999 (2000–2022) is mainly driven by the RPEs under the Type1 (Type1 and Type2 together). The reduced RPE coverage rate and occurrence hours under the monsoonal synoptic types (Type 1 and Type 2) dominate the weakened diurnal variation of the RPE precipitation amount during 2000–2022 compared with 1980–1999.

Overall, the cluster analysis reasonably reveals the diurnal and sub-seasonal variations, long-term trends, and formation mechanisms of the summer RPEs over the MLYRB under different synoptic types. Our results also emphasize the importance of RPEs for the total precipitation over the MLYRB in summer. Moreover, although this study demonstrates the basic features of summer RPEs over the MLYRB under different dominant synoptic types and their differences, the detailed dynamical processes responsible for this phenomenon require further study.

## Data Availability Statement

The hourly geopotential height, *u* and *v* components of wind speed, and specific humidity are accessed from ERA5 (Hersbach et al., 2020).

**Acknowledgments**

This study is funded by the National Natural Science Foundation of China under Grants U2342207, the Postgraduate Research and Practice Innovation Program of Jiangsu Province (No. 206 in 2024), and the Jiangsu Collaborative Innovation Center for Climate Change.

## References

Allan, R. P., Barlow, M., Byrne, M. P., Cherchi, A., Douville, H., Fowler, H. J., et al. (2020). Advances in understanding large-scale responses of the water cycle to climate change. *Annals of the New York Academy of Sciences*, *1472*(1), 49–75. https://doi.org/10.1111/nyas.14337

Caliński, T., & Harabasz, J. (1974). A dendrite method for cluster analysis. *Communications in Statistics - Theory and Methods*, *3*(1), 1–27. https://doi.org/10.1080/03610927408827101

Cao, F., Gao, T., Dan, L., Ma, Z., Chen, X., Zou, L., & Zhang, L. (2019). Synoptic-scale atmospheric circulation anomalies associated with summertime daily precipitation extremes in the middle–lower reaches of the Yangtze River Basin. *Climate Dynamics*, *53*(5–6), 3109–3129. https://doi.org/10.1007/s00382-019-04687-3

Cavalcanti, I. F. A. (2012). Large scale and synoptic features associated with extreme precipitation over South America: A review and case studies for the first decade of the 21st century. *Atmospheric Research*, *118*, 27–40. https://doi.org/10.1016/j.atmosres.2012.06.012

Chen, G., Sha, W., Iwasaki, T., & Ueno, K. (2012). Diurnal variation of rainfall in the Yangtze River Valley during the spring-summer transition from TRMM measurements. *Journal of Geophysical Research*, *117*(D6). https://doi.org/10.1029/2011JD017056

Chen, Y., & Zhai, P. (2016). Mechanisms for concurrent low-latitude circulation anomalies responsible for persistent extreme precipitation in the Yangtze River Valley. *Climate Dynamics*, *47*(3–4), 989–1006. https://doi.org/10.1007/s00382-015-2885-6

Chen, Y., Zhang, A., Zhang, Y., Cui, C., Wan, R., Wang, B., & Fu, Y. (2020). A heavy precipitation event in the Yangtze River Basin led by an eastward moving Tibetan Plateau cloud system in the summer of 2016. *Journal of Geophysical Research: Atmospheres*, *125*(15). https://doi.org/10.1029/2020JD032429

Dagan, G., & Stier, P. (2020). Constraint on precipitation response to climate change by combination of atmospheric energy and water budgets. *npj Climate and Atmospheric Science*, *3*(1), 34. https://doi.org/10.1038/s41612-020-00137-8

Dai, P., Nie, J., Yu, Y., & Wu, R. (2024). Constraints on regional projections of mean and extreme precipitation under warming. *Proceedings of the National Academy of Sciences*, *121*(11), e2312400121. https://doi.org/10.1073/pnas.2312400121

Donath, W. E., & Hoffman, A. J. (1973). Lower bounds for the partitioning of graphs. *IBM Journal of Research and Development*, *17*(5), 420–425. https://doi.org/10.1147/rd.175.0420

Emanuel, K. (2005). Increasing destructiveness of tropical cyclones over the past 30 years. *Nature*, *436*(7051), 686–688. https://doi.org/10.1038/nature03906

Ester, M., Kriegel, H.-P., Sander, J., & Xu, X. (1996). A density-based algorithm for discovering clusters in large spatial databases with noise, paper presented at kdd.

Gao, T., Zou, L., Cao, F., & Zhan, J. (2023). Impacts of tropical cyclones on summertime short-duration precipitation extremes over the middle-lower reaches of the Yangtze River valley. *Atmospheric Research*, *282*, 106520. https://doi.org/10.1016/j.atmosres.2022.106520

Gu, L., Chen, J., Yin, J., Xu, C. Y., & Zhou, J. (2020). Responses of precipitation and runoff to climate warming and implications for future drought changes in China. *Earth's Future*, *8*(10), e2020EF001718. https://doi.org/10.1029/2020EF001718

Guan, W., Hu, H., Ren, X., & Yang, X.-Q. (2019). Subseasonal zonal variability of the western Pacific subtropical high in summer: Climate impacts and underlying mechanisms. *Climate Dynamics*, *53*(5–6), 3325–3344. https://doi.org/10.1007/s00382-019-04705-4

Guo, J., Su, T., Li, Z., Miao, Y., Li, J., Liu, H., et al. (2017). Declining frequency of summertime local-scale precipitation over eastern China from 1970 to 2010 and its potential link to aerosols. *Geophysical Research Letters*, *44*(11), 5700–5708. https://doi.org/10.1002/2017GL073533

Hersbach, H., Bell, B., Berrisford, P., Hirahara, S., Horányi, A., Muñoz-Sabater, J., et al. (2020). The ERA5 global reanalysis. *Quarterly Journal of the Royal Meteorological Society*, *146*(730), 1999–2049. [Dataset]. https://doi.org/10.1002/qj.3803

Hu, X., & Yuan, W. (2021). Evaluation of ERA5 precipitation over the eastern periphery of the Tibetan plateau from the perspective of regional rainfall events. *International Journal of Climatology*, *41*(4), 2625–2637. https://doi.org/10.1002/joc.6980

Hu, X., Yuan, W., Yu, R., & Zhang, M. (2020). The evolution process of warm season intense regional rainfall events in Yaan. *Climate Dynamics*, *54*(7–8), 3245–3258. https://doi.org/10.1007/s00382-020-05168-8

Hu, Y., Lin, Y., Deng, Y., & Bao, J. (2023). Summer extreme rainfall over the middle and lower reaches of Yangtze River: Role of synoptic patterns in historical changes and future projections. *Journal of Geophysical Research: Atmospheres*, *128*(24). https://doi.org/10.1029/2023JD039608

Huang, R., Liu, Y., & Feng, T. (2013). Interdecadal change of summer precipitation over Eastern China around the late-1990s and associated circulation anomalies, internal dynamical causes. *Chinese Science Bulletin*, *58*(12), 1339–1349. https://doi.org/10.1007/s11434-012-5545-9

Korell, L., Auge, H., Chase, J. M., Harpole, W. S., & Knight, T. M. (2021). Responses of plant diversity to precipitation change are strongest at local spatial scales and in drylands. *Nature Communications*, *12*(1), 2489. https://doi.org/10.1038/s41467-021-22766-0

Kukulies, J., Chen, D., & Curio, J. (2021). The role of mesoscale convective systems in precipitation in the Tibetan Plateau region. *Journal of Geophysical Research: Atmospheres*, *126*(23), e2021JD035279. https://doi.org/10.1029/2021JD035279

Li, H.-S., Ding, Y.-H., & Liu, Y.-J. (2024). New characteristics of Meiyu precipitation changes in the middle and lower reaches of the Yangtze River since 2000. *Frontiers in Climate*, *6*, 1372460. https://doi.org/10.3389/fclim.2024.1372460

Li, L., Li, J., & Yu, R. (2020a). Characteristics of summer regional rainfall events over Ili river valley in northwest China. *Atmospheric Research*, *243*, 104996. https://doi.org/10.1016/j.atmosres.2020.104996

Li, P., Furtado, K., Zhou, T., Chen, H., Li, J., Guo, Z., & Xiao, C. (2020b). The diurnal cycle of East Asian summer monsoon precipitation simulated by the Met Office Unified Model at convection-permitting scales. *Climate Dynamics*, *55*(1–2), 131–151. https://doi.org/10.1007/s00382-018-4368-z

Li, W., Sun, B., Wang, H., Zhou, B., Li, H., Xue, R., et al. (2023). Anthropogenic impact on the severity of compound extreme high temperature and drought/rain events in China. *npj Climate and Atmospheric Science*, *6*(1), 79. https://doi.org/10.1038/s41612-023-00413-3

Li, X., Zhang, K., Gu, P., Feng, H., Yin, Y., Chen, W., & Cheng, B. (2021). Changes in precipitation extremes in the Yangtze River Basin during 1960–2019 and the association with global warming, ENSO, and local effects. *Science of the Total Environment*, *760*, 144244. https://doi.org/10.1016/j.scitotenv.2020.144244

Li, Z., Li, W., & Zhang, A. (2022). Analysis of diurnal variation characteristics of precipitation over South China before typhoon landfall. *Journal of Tropical Oceanography*, *41*(2), 26–37. https://doi.org/10.11978/2021045

Liu, Y., Huang, D., Zhu, J., & Cheng, C. S. (2023). The Quadrupole precipitation pattern over eastern China and its associated atmospheric circulations and ocean conditions. *Journal of Climate*, *36*(18), 6561–6575. https://doi.org/10.1175/JCLI-D-22-0075.1

Ma, J., & Yao, X. (2015). Statistical analysis of the shear lines and torrential rains over the Yangtze-Huaihe river region during June–July in 1981–2013. Acta Meteorol. *Sin*, *73*(5), 883–894. https://doi.org/10.11676/qxxb2015.065

Markonis, Y., Papalexiou, S., Martinkova, M., & Hanel, M. (2019). Assessment of water cycle intensification over land using a multisource global gridded precipitation dataset. *Journal of Geophysical Research: Atmospheres*, *124*(21), 11175–11187. https://doi.org/10.1029/2019JD030855

Muller, C. J., & O'Gorman, P. (2011). An energetic perspective on the regional response of precipitation to climate change. *Nature Climate Change*, *1*(5), 266–271. https://doi.org/10.1038/nclimate1169

Muszynski, G., Kashinath, K., Kurlin, V., Wehner, M., & Prabhat (2019). Topological data analysis and machine learning for recognizing atmospheric river patterns in large climate datasets. *Geoscientific Model Development*, *12*(2), 613–628. https://doi.org/10.5194/gmd-12-613-2019

Pedregosa, F., Varoquaux, G., Gramfort, A., Michel, V., Thirion, B., Grisel, O., et al. (2011). Scikit-learn: Machine learning in Python. *Journal of Machine Learning Research*, *12*, 2825–2830.

Qi, Y., Li, T., Zhang, R., & Chen, Y. (2019). Interannual relationship between intensity of rainfall intraseasonal oscillation and summer-mean rainfall over Yangtze River Basin in eastern China. *Climate Dynamics*, *53*(5), 3089–3108. https://doi.org/10.1007/s00382-019-04680-w

Qin, L., Zhu, L., Liu, B., Li, Z., Tian, Y., Mitchell, G., et al. (2024). Global expansion of tropical cyclone precipitation footprint. *Nature Communications*, *15*(1), 4824. https://doi.org/10.1038/s41467-024-49115-1

Ren, X., Yang, X.-Q., & Sun, X. (2013). Zonal oscillation of western Pacific subtropical high and subseasonal SST variations during Yangtze persistent heavy rainfall events. *Journal of Climate*, *26*(22), 8929–8946. https://doi.org/10.1175/JCLI-D-12-00861.1

Salcedo-Sanz, S., Pérez-Aracil, J., Ascenso, G., Del Ser, J., Casillas-Pérez, D., Kadow, C., et al. (2024). Analysis, characterization, prediction, and attribution of extreme atmospheric events with machine learning and deep learning techniques: A review. *Theoretical and Applied Climatology*, *155*(1), 1–44. https://doi.org/10.1007/s00704-023-04571-5

Schubert, E., Sander, J., Ester, M., Kriegel, H. P., & Xu, X. (2017). DBSCAN revisited, revisited: Why and how you should (still) use DBSCAN. *ACM Transactions on Database Systems*, *42*(3), 1–21. https://doi.org/10.1145/3068335

Schumacher, R. S., & Rasmussen, K. L. (2020). The formation, character and changing nature of mesoscale convective systems. *Nature Reviews Earth and Environment*, *1*(6), 300–314. https://doi.org/10.1038/s43017-020-0057-7

Tan, X., Wu, X., Huang, Z., Fu, J., Tan, X., Deng, S., et al. (2023). Increasing global precipitation whiplash due to anthropogenic greenhouse gas emissions. *Nature Communications*, *14*(1), 2796. https://doi.org/10.1038/s41467-023-38510-9

Tang, X., Cai, Q., Fang, J., & Tan, Z. M. (2019). Land–sea contrast in the diurnal variation of precipitation from landfalling tropical cyclones. *Journal of Geophysical Research: Atmospheres*, *124*(22), 12010–12021. https://doi.org/10.1029/2019JD031454

Tang, Y., Huang, A., Wu, P., Huang, D., Xue, D., & Wu, Y. (2021). Drivers of summer extreme precipitation events over East China. *Geophysical Research Letters*, *48*(11), e2021GL093670. https://doi.org/10.1029/2021GL093670

Von Luxburg, U. (2007). A tutorial on spectral clustering. *Statistics and Computing*, *17*(4), 395–416. https://doi.org/10.1007/s11222-007-9033-z

Wang, G., Wang, D., Trenberth, K. E., Erfanian, A., Yu, M., Bosilovich, M. G., & Parr, D. T. (2017). The peak structure and future changes of the relationships between extreme precipitation and temperature. *Nature Climate Change*, *7*(4), 268–274. https://doi.org/10.1038/nclimate3239

Wang, H., Sun, J., Fu, S., & Zhang, Y. (2021). Typical circulation patterns and associated mechanisms for persistent heavy rainfall events over Yangtze-Huaihe River Valley during 1981–2020. *Advances in Atmospheric Sciences*, *38*(12), 2167–2182. https://doi.org/10.1007/s00376-021-1194-8

Wang, S., Ma, X., Zhou, S., Wu, L., Wang, H., Tang, Z., et al. (2023). Extreme atmospheric rivers in a warming climate. *Nature Communications*, *14*(1), 3219. https://doi.org/10.1038/s41467-023-38980-x

Wang, X., Luo, M., Wu, S., Ning, G., Liu, Z., Wang, S., et al. (2022). Spatiotemporal evolution patterns of contiguous extreme precipitation events across China from a 3D perspective. *Geophysical Research Letters*, *49*(16), e2022GL098840. https://doi.org/10.1029/2022GL098840

Wei, W., Zhang, R., Wen, M., Rong, X., & Li, T. (2014). Impact of Indian summer monsoon on the South Asian High and its influence on summer rainfall over China. *Climate Dynamics*, *43*(5–6), 1257–1269. https://doi.org/10.1007/s00382-013-1938-y

Wen, N., Liu, Z., & Li, L. (2019). Direct ENSO impact on East Asian summer precipitation in the developing summer. *Climate Dynamics*, *52*(11), 6799–6815. https://doi.org/10.1007/s00382-018-4545-0

Wu, M., Zhang, R.-H., Hu, J., & Zhi, H. (2024). Synergistic interdecadal evolution of precipitation over Eastern China and the Pacific decadal oscillation during 1951–2015. *Advances in Atmospheric Sciences*, *41*(1), 53–72. https://doi.org/10.1007/s00376-023-3011-z

Wu, X., Tan, X., Liu, B., Chen, H., & Chen, X. (2022). Fronts and cyclones associated with changes in the total and extreme precipitation over China. *Journal of Climate*, *35*(13), 4131–4146. https://doi.org/10.1175/JCLI-D-21-0467.1

Wu, Y., Huang, A., Huang, D., Chen, F., Yang, B., Zhou, Y., et al. (2018). Diurnal variations of summer precipitation over the regions east to Tibetan Plateau. *Climate Dynamics*, *51*(11–12), 4287–4307. https://doi.org/10.1007/s00382-017-4042-x

Wu, Y., Yin, X., Zhou, G., Bruijnzeel, L. A., Dai, A., Wang, F., et al. (2024). Rising rainfall intensity induces spatially divergent hydrological changes within a large river basin. *Nature Communications*, *15*(1), 823. https://doi.org/10.1038/s41467-023-44562-8

Xu, X., Huang, A., Huang, D., Zhang, Y., Gu, C., Cai, S., et al. (2023). What are the dominant synoptic patterns leading to the summer regional hourly extreme precipitation events over central-eastern Tibetan plateau and Sichuan basin? *Geophysical Research Letters*, *50*(5). https://doi.org/10.1029/2022gl102342

Xue, M., Luo, X., Zhu, K., Sun, Z., & Fei, J. (2018). The controlling role of boundary layer inertial oscillations in Meiyu frontal precipitation and its diurnal cycles over China. *Journal of Geophysical Research: Atmospheres*, *123*(10), 5090–5115. https://doi.org/10.1029/2018JD028368

Yang, J., Bao, Q., Wang, B., Gong, D.-Y., He, H., & Gao, M.-N. (2014). Distinct quasi-biweekly features of the subtropical East Asian monsoon during early and late summers. *Climate Dynamics*, *42*(5–6), 1469–1486. https://doi.org/10.1007/s00382-013-1728-6

Yao, R., Zhang, S., Sun, P., Bian, Y., Yang, Q., Guan, Z., & Zhang, Y. (2022). Diurnal variations in different precipitation duration events over the Yangtze River Delta Urban agglomeration. *Remote Sensing*, *14*(20), 5244. https://doi.org/10.3390/rs14205244

Yu, R., Chen, H., & Sun, W. (2015). The definition and characteristics of regional rainfall events demonstrated by warm season precipitation over the Beijing plain. *Journal of Hydrometeorology*, *16*(1), 396–406. https://doi.org/10.1175/JHM-D-14-0086.1

Yu, R., Li, J., Chen, H., & Yuan, W. (2014). Progress in studies of the precipitation diurnal variation over contiguous China. *Journal of Meteorological Research*, *28*(5), 877–902. https://doi.org/10.1007/s13351-014-3272-7

Yu, R., Xu, Y., Zhou, T., & Li, J. (2007). Relation between rainfall duration and diurnal variation in the warm season precipitation over central eastern China. *Geophysical Research Letters*, *34*(13). https://doi.org/10.1029/2007GL030315

Zeng, J., Huang, A., Wu, P., Huang, D., Zhang, Y., Tang, J., et al. (2023). Typical synoptic patterns responsible for summer regional hourly extreme precipitation events over the middle and lower Yangtze River basin, China. *Geophysical Research Letters*, *50*(17), e2023GL104829. https://doi.org/10.1029/2023GL104829

Zhang, D., Huang, Y., Zhou, B., & Wang, H. (2021). Is there interdecadal variation in the South Asian high? *Journal of Climate*, *34*(20), 8089–8103. https://doi.org/10.1175/JCLI-D-21-0059.1
Zhang, M., Zhang, Y., Tian, Y., Xie, D., Cao, Y., Mei, Y., et al. (2024). On the moisture transport regimes for extreme precipitation over North China. *Atmospheric Research*, *300*, 107254. https://doi.org/10.1016/j.atmosres.2024.107254
Zhang, Q., Han, J., & Yang, Z. (2021). Spatiotemporal characteristics of regional precipitation events in the Jing-Jin-Ji region during 1989–2018. *International Journal of Climatology*, *41*(2), 1190–1198. https://doi.org/10.1002/joc.6786
Zhang, Q., Xu, C.-Y., Zhang, Z., Chen, Y. D., Liu, C.-l., & Lin, H. (2008). Spatial and temporal variability of precipitation maxima during 1960–2005 in the Yangtze River basin and possible association with large-scale circulation. *Journal of Hydrology*, *353*(3–4), 215–227. https://doi.org/10.1016/j.jhydrol.2007.11.023
Zhao, Y., Li, J., & Li, P. (2023). Diurnal cycle of precipitation over the southeastern Tibetan Plateau and surrounding regions: Insights from intensity–frequency structure. *International Journal of Climatology*, *43*(7), 3284–3297. https://doi.org/10.1002/joc.8029
Zhu, S., Liu, C., Cao, J., & Lavigne, T. (2023). Diurnal precipitation features over complex terrains along the Yangtze River in China based on long-term TRMM and GPM radar products. *Remote Sensing*, *15*(13), 3451. https://doi.org/10.3390/rs15133451
Zhu, Y., Wang, H., Zhou, W., & Ma, J. (2011). Recent changes in the summer precipitation pattern in East China and the background circulation. *Climate Dynamics*, *36*(7–8), 1463–1473. https://doi.org/10.1007/s00382-010-0852-9